Acta Biomaterialia 187 (2024) 352–365

Contents lists available at ScienceDirect

Acta Biomaterialia

journal homepage: www.elsevier.com/locate/actbio

Full length article

Brain biodistribution of myelin nanovesicles with targeting potential for multiple sclerosis

Pasquale Picone[a,1,*], Fabio Salvatore Palumbo[b,1], Francesco Cancilla[b], Antonella Girgenti[a], Patrizia Cancemi[b], Vera Muccilli[c], Antonella Di Francesco[c], Maura Cimino[e], Chiara Cipollina[a,e], Marzia Soligo[d], Luigi Manni[d], Gianluca Sferrazza[d,g], Luca Scalisi[f], Domenico Nuzzo[a,*]

[a] Istituto per la Ricerca e l'Innovazione Biomedica, CNR, via U. La Malfa 153, Palermo 90146, Italy
[b] Dipartimento di Scienze e Tecnologie Biologiche Chimiche e Farmaceutiche, Università di Palermo, Viale delle Scienze, Palermo 90128, Italy
[c] Dipartimento di Scienze Chimiche, Università degli Studi di Catania, Viale A. Doria, 6, Catania I-95125, Italy
[d] Istituto di Farmacologia Traslazionale, CNR, Via Fosso del Cavaliere 100, Roma 00133, Italy
[e] Fondazione RiMED, Palermo, Italy
[f] Centro Medico di Fisioterapia Villa Sarina, Alcamo, Palermo 91011, Italy
[g] Dipartimento di Scienze Biomediche, CNR, Roma 00185, Italy

ARTICLE INFO

Article history:
Received 18 April 2024
Revised 6 August 2024
Accepted 12 August 2024
Available online 17 August 2024

Keywords:
Nanovesicles
Neuroinflammation
Multiple sclerosis
Brain delivery

ABSTRACT

Multiple sclerosis (MS) is a complex autoimmune disease with multiple players. In particular, peripheral (myelin-reactive CD4+ T lymphocytes) and central immune cells (microglia) are involved in the neuroinflammatory process and are found in MS brain lesions. New nanotechnological approaches that can cross the blood-brain barrier and specifically target the key players in the disease using biocompatible nanomaterials with low immunoreactivity represent an important challenge. To this end, nanoparticles and nanovesicles have been studied to induce immune tolerance to a wide range of myelin-derived antigens as potential approaches against MS. To this aim, we extracted myelin from bovine brain and produced myelin-based nanovesicles (MyVes) by nanoprecipitation. MyVes have a diameter of about 100 nm, negative zeta potential and contain the typical proteins of the myelin sheath. The results showed that MyVes are not cytotoxic, are hemocompatibile and do not induce an inflammatory response. *In vitro* experiments showed that MyVes are specifically taken up by microglial cells and are able to induce the expression of the anti-inflammatory cytokine IL-4. In addition, we have used biodistribution experiments to show that MyVes are able to reach the brain after intranasal administration. Finally, MyVes induced the production of the anti-inflammatory cytokines IL-10 and IL-4 in peripheral blood mononuclear cells isolated from MS patients. Taken together, these data provide proof of concept that MyVes may represent a safe nanosystem capable of promoting anti-inflammatory effects by modulating both central and peripheral immune cells to treat neuroinflammation in MS.

Statement of significance

Recently, nanoparticles and nanovesicles have been investigated as potential approaches for the treatment of neurodegenerative diseases. We propose the use of myelin nanovesicles (MyVes) as a potential application to counteract neuroinflammation in multiple sclerosis (MS). Approximately 2.8 million people worldwide are estimated to live with MS. It is an autoimmune disease directed toward various myelin-derived antigens. Both peripheral immune cells (lymphocytes) and central immune cells (microglia) actively contribute to MS brain lesions. MyVes, due to their myelin nature, specific characteristics (size, zeta potential, and presence of myelin proteins), biocompatibility, and ability to cross the blood-brain barrier,

* Corresponding authors.
E-mail addresses: pasquale.picone@cnr.it (P. Picone), domenico.nuzzo@cnr.it (D. Nuzzo).
[1] These authors contributed equally to this work.

https://doi.org/10.1016/j.actbio.2024.08.016

could represent the first nanosystem capable of promoting anti-inflammatory actions by modulating both central and peripheral immune cells to treat neuroinflammation in MS.

1. Introduction

Multiple sclerosis (MS) is an autoimmune disease of the central nervous system (CNS) in which an inflammatory process leads to the destruction of myelin, resulting in neuronal death, neurodegeneration and disability [1]. MS has a preclinical phase, a radiologically isolated syndrome (RIS), followed by a relapsing-remitting stage (RRMS), which can later progress to secondary progressive disease (SPMS) [2]. RRMS is associated with inflammation and demyelination, mainly in the white matter [1,2]. The first event in the pathogenesis of MS is a breakdown of tolerance leading to the activation of systemic naive myelin-specific T cells that infiltrate the CNS [1,3]. Although the detailed mechanisms are not fully understood, a dominant hypothesis is that the loss of immune tolerance to myelin proteins, such as Myelin Basic Protein (MBP), Proteolipid Protein (PLP), and Myelin Oligodendrocyte Glycoprotein (MOG), leads to the recruitment of myelin-specific CD4+ T cells, resulting in myelin damage [4,5]. This hypothesis is mainly based on animal models of MS and not on MS patients [4]. In fact, in MS patients, the pattern of recognized autoantigens progressively increases over the course of the disease, due to the phenomenon known as "epitope spreading" [5,6]. Furthermore, the disease is highly heterogeneous, involving multiple autoantigens that can vary between patients depending on age, disease duration, genetic characteristics and environmental factors [4,7]. In addition, the destruction of myelin in the CNS in MS patients is associated with activated microglia, which is involved in the pathogenesis of the disease [8]. In fact, more than 80% of MS-specific genes identified in active demyelinating lesions are associated with microglia and T-cell-mediated inflammation [9]. Microglia can have a dual effect, promoting remyelination, phagocytosis of debris and tissue repair through the expression of anti-inflammatory molecules. On the other hand, as antigen-presenting cells (APCs), microglia secrete pro-inflammatory molecules that can damage the myelin sheath and/or oligodendrocytes. In addition, microglia are involved in interacting with other immune cells and leading to T cell activation during demyelination and remyelination in MS [8,9]. In addition to immunosuppressive drugs (which largely suppress the immune system), other approaches have been explored that target immune cells to inhibit their passage across the blood-brain barrier (BBB) and induce immune tolerance [2,10]. Antigen-specific immunotherapies aim to restore immune tolerance without suppressing overall immune surveillance against microbes and cancer; this is the holy grail for MS treatment [4]. Previous studies with myelin peptides (antigens-Ags) (full-length protein or fragments) have demonstrated their safety, feasibility and efficacy in inducing antigen-specific immune tolerance in animal models of MS [4,5]. Antigen-specific immunotherapies are based on the introduction of self-antigens into APCs that (I) act directly on effector T cells, resulting in immunological anergy and deletion of pathogenic T cell clones, and (II) activate antigen-specific regulatory T cells that secrete anti-inflammatory cytokines [5]. Recently, nanoparticles and nanovesicles have been investigated as effective tools for the induction of immune tolerance through the delivery of specific myelin antigens or immunomodulatory drugs or through an antigen-drug conjugate for the treatment of neurodegenerative diseases such as MS [5,11–14]. The use of nanosystems is expected to provide unique opportunities to: (i) improve drug solubility and bioavailability; (ii) enable targeted delivery and controlled release; (iii) increase effective routes of administration; and (iv) reduce toxicity [11]. Therefore, the first challenge for antigen-specific immune tolerance is that the target antigens in MS patients are unknown and remain to be identified [5]. In this regard, it may be useful to pursue nanotherapeutic strategies targeting a wider range of epitopes [11]. To address these issues, we propose a therapeutic strategy based on the biofabrication of myelin-based nanovesicles (MyVes) containing multiple myelin Ags [15]. Oral treatment with bovine myelin was attempted in 1993, but this administration did not significantly improve the disease in MS patients [16]. The ineffectiveness of the treatment could be related to the mode of administration, which, being oral, could lead to alteration of the myelin itself and the proteins present in it. We have previously shown that MyVes are approximately 100 nm in size, have a negative zeta potential and naturally contain multiple myelin Ags [15]. Furthermore, MyVes cross the BBB model *in vitro*, reach the white matter and interact specifically with microglial cells [15].

The aim of the present study was to characterize the safety profile of MyVes through a combination of *in vitro* cytotoxicity, hemocompatibility and immunocompatibility assays. Furthermore, the results presented here indicate that MyVes reaches the brain via intranasal administration, modulates microglial cells, and induces an immunomodulatory effect in peripheral blood mononuclear cells (PBMCs) isolated from MS patients. Therefore, these data provide proof of concept that MyVes could represent a system capable of promoting anti-inflammatory effects by modulating both central (microglia) and peripheral immune cells (lymphocytes) to treat neuroinflammation in MS.

2. Material and methods

2.1. Materials and instruments

Dimethyl sulfoxide (DMSO), ethanol, Atto 633 NHS ester, sodium chloride (NaCl), potassium dihydrogen phosphate, dipotassium hydrogen phosphate, and Dulbecco's phosphate buffered saline (DPBS) were acquired from Sigma-Aldrich (Italy). Alexa Fluor 568 NHS ester was acquired from Thermo Fisher Scientific (Waltham, MA). Vigorous agitation was performed using an Ultraturrax (T 25, Janke & Kunkel Ika-Labortechnik). The nanoparticle size, dimensional distribution and Z-potential were determined using a Zetasizer Nano ZS (Malvern Instruments, Malvern, UK). The measurements were performed at 25°C and at a fixed angle of 173°. Ultracentrifugation was performed using the Optima XPN-100 Ultracentrifuge (Beckman Coulter). Centrifugation was performed using an Eppendorf Centrifuge 5804 R. The solutions were dried using an Eppendorf Concentrator Plus and mixed using an Eppendorf ThermoMixer C. The UV spectra were recorded using a Shimadzu UV-2401PC spectrophotometer. Scanner fluorescence of Typhoon FLA 9500 (GE Healthcare Life Sciences). Opera high-content screening system (PerkinElmer). Antiprotease (Amersham Biosciences, Milan, Italy) and phosphatase cocktail inhibitors (cocktail II and III; Sigma-Aldrich, Milan, Italy). Atomic Force Microscopy (AFM) images were obtained on a FAST-SCAN microscope equipped with a closed-loop scanner. The analysis was performed in tapping mode using a FAST-SCAN-A probe with an apical radius of 5 nm operating at 1400 kHz. The sample was prepared by depositing 10 µL of a 10-3 mg/mL aqueous dispersion of MyVes on MICA sub-

strates. After standing on the substrates for about 1 min, the sample solution was blown off with a flow of N2.

2.2. Isolation and extraction of bovine myelin

The bovine brain, being material for food use, was purchased at the slaughterhouse and transported on ice immediately after removal. Myelin isolation and extraction were performed according to the protocol of Picone et al. [15]. Briefly, the white matter of the brain (80–100 mg), rich in myelinated nerve fibers, was quickly removed and homogenized in 0.32 M sucrose with 10% antiprotease and phosphatase inhibitors with a Dounce on ice. The homogenate was mixed with 2 M sucrose and 0.1 mM $CaCl_2$, transferred to an ultracentrifuge tube, and ultracentrifuged at 127,000 Relative Centrifugal Force (RCF) for 3 h at 4°C. The floating myelin layer on top was collected and washed twice in deionized water by centrifugation at 14,000 rpm for 15 min. Subsequently, the pellet containing the myelin extract was cold lyophilized.

2.3. Myelin nanovesicles production, labeling with fluorescent probes and characterization

Myelin nanovesicles (MyVes) were obtained by nanoprecipitation of a myelin solution, according to a previously reported procedure with some modifications [15]. Firstly, myelin extract powder was dispersed at a concentration of 2 mg/mL in DMSO and sonicated (30 min at 35 kHz). Then, MyVes was produced according to the nanoprecipitation procedure using the solvent injection technique. Specifically, 1 mL of myelin solution in DMSO (2 mg/mL) was added dropwise to 20 mL of ultrapure water with vigorous agitation (Ultraturrax, 8000 rpm, 15 min). After agitation, the product was purified by repeated ultracentrifugation (30 min, 50,000 rpm) to remove the solvent, redispersed in 2 mL of ultrapure water, and freeze-dried.

Myelin powder was dissolved in DPBS buffer at 1 mg/mL to prepare the non-nanostructured myelin solution. For fluorescence labeling, 50 µL of Atto 633 NHS ester in DMSO (2 mg/mL) was added to 2 mL of MyVes re-dispersed in DPBS (2 mg/mL). The mixture was allowed to react for 2 h in the dark, followed by ultracentrifugation (30 min, 50,000 rpm). The product was washed three times with ultrapure water and ultracentrifuged (30 min at 50,000 rpm). Finally, MyVes were redispersed in 2 mL of ultrapure water and freeze-dried. For the uptake test, MyVes were labeled with Alexa Fluor 568 NHS ester. In particular, 50 µL of Alexa Fluor 568 NHS ester in DMSO (2 mg/mL) was added to 2 mL of redispersed MyVes in phosphate buffer at pH 8 (2 mg/mL). After 1 h of incubation in the dark, the dispersion was ultracentrifuged (30 min, 50,000 rpm) and the product was washed three times with ultrapure water. The MyVes were then ultracentrifuged (30 min, 50,000 rpm), redispersed in 2 mL of ultrapure water, and freeze-dried. Size, polydispersity index (PDI) and Z potential of MyVes were measured on filtered dispersions (cut-off: 5 µm) obtained after nanoprecipitation and from the freeze-dried product redispersed in ultrapure water (0.1 mg/mL) and sonicated (30 min, 35 kHz). To assay stability of vesicles, freeze-dried product was redispersed in DMEM buffer at pH 7.4 and analyzed trough dynamic light scattering at 37°C for 48 h. Moreover, in order to detect possible leakage of probe from the marked MyVes, 2 mg of freeze-dried particles were redispersed in 1 ml of water as previously described. The entire volume of aqueous dispersion was the loaded in a floating dialysis bag (3000 Da Cut-off) and exhaustively dialyzed for 3 days against 5 ml of DPBS. At predetermined time point, 1, 24 and 36 h 1 ml of external medium was analyzed by florescence spectroscopy (ATTO633 excitation 629 nm and emission 650 nm) in order to detect the amount of fluorophore released.

FluoroMyelin™ Green (Thermo Fisher Scientific™) fluorescent myelin staining enables rapid and selective labeling of myelin in brain cryosections, MyVes and non-nanostructured myelin solution (1mg/mL) in a single 20-minute labeling step (staining solution by diluting the stock solution 300-fold in PBS) followed by 3 washes in PBS. FluoroMyelin™ Green excitation/emission 479/598 nm. Fluorescence was analyzed using a fluorometer (GLOMAX Promega), a Typhoon FLA 9500 fluorescence scanner (GE Healthcare Life Sciences), and a fluorescence microscope (Axio Scope 2 microscope; Zeiss).

2.4. Proteomic analysis

2.4.1. Sample treatment

The MyVes pellet was rinsed with 50 µL of 0.05 M ammonium bicarbonate, pH 8.2, and 0.1% RapiGest®. The solution was mixed at 55°C for 20 min. The protein concentration of the protein fraction was determined by a fluorometric assay using the Qubit Protein Assay kit and a Qubit 1.0 Fluorometer (ThermoFisher Scientific, Milan, Italy) [17]. Finally, a volume containing 4 µg of protein mixture was purified from non-protein contaminating molecules using the PlusOne 2-D Clean-Up kit (GE Healthcare Life Sciences, Milan, Italy) according to the manufacturer's instructions. The desalted protein pellet was resuspended in 40 µL of 50 mM ammonium bicarbonate and incubated at 4°C for 15 min. Next, 40 µL of 0.2% RapiGest SF (Waters, Milan, Italy) in 50 mM ammonium bicarbonate was added and the samples were incubated at 4°C for 30 min. Finally, the sample was reduced adding 11 µg of DTT (3 h, 20°C), alkylated with 27 µg of IAA (1 h, in the dark at 20 °C), and digested with porcine trypsin (Sequencing Grade modified Trypsin Porcine, lyophilized, Promega) at an enzyme-substrate ratio of 1:50 (overnight, 37°C). The peptide mixture was then diluted to a final concentration of 25 ng/µL.

2.4.2. Mass spectrometric analysis

Mass spectrometry data were acquired following the procedure described by Picone et al. 2021 [15].

2.4.3. Database search and protein identification

Triplicate mass spectrometry data were processed using PEAKS X de novo sequencing software (v. 10.0; Bioinformatics Solutions Inc., Waterloo, ON, Canada). MS data were searched against the SwissProt database and restricted to the reviewed Bos taurus entries (936, release January 2023). A database search was performed using the following parameters: (i) full tryptic peptides with a maximum of three missed cleavage sites, (ii) oxidation of methionine, transformation of N-terminal glutamine and N-terminal glutamic acid residue in the pyroglutamic acid form, and deamidation of asparagine and glutamine as variable modifications, and (iii) carbamidomethylation of cysteine as a fixed modification. The precursor mass tolerance threshold was 10 ppm and the maximum fragment mass error was set to 0.6 Da. Peptide Spectral Matches (PSMs) were validated using a target decoy PSM valve node based on q-values at a False Discovery Rate (FDR) $\leq$ 1. PEAKS score thresholds for PSMs were set to achieve, for each database search, FDR values for PSMs, peptide sequences, and proteins identified below 1. A protein was considered to be identified if a minimum of two peptides (one unique peptide) matched. Proteins containing the same peptides that could not be differentiated based on MS/MS analysis alone were grouped to satisfy the principles of parsimony (Occam razor).

2.5. Cell cultures

SH-SY5Y cells, generously provided by Dr. Venera Cardile, University of Catania, Italy, were cultured in T25 tissue-culture flasks.

Complete Dulbecco's Modified Eagle's medium (DMEM) and F12 (DMEM/F12; 1:1) were supplemented with 10% fetal bovine serum (FBS) (GIBCO Invitrogen, Milan, Italy), 100 U/ml penicillin, 100 U/ml streptomycin, and 2 mM L-glutamine.

BV2 microglial cells were cultured in DMEM (GIBCO, Carlsbad, CA, USA) supplemented with 10% FBS (Gibco), 100 U/ml penicillin, 100 U/ml streptomycin, and 2 mM l-glutamine.

PBMCs were isolated from heparinized blood of donors by Ficoll-Paque Plus (GE Healthcare Bio-Sciences AB) and cultured in complete RPMI 1640 medium supplemented with 10% heat-inactivated fetal calf serum (Gibco), 2 mM L-glutamine, and 100 U/ml penicillin/streptomycin at 37°C.

2.6. Cell viability and cytotoxicity assays

Cell viability was measured using the MTS assay (Promega). MTS [3-(4,5- dimethylthiazol-2-yl)-5-(3carboxymethoxyphenyl)-2-(4-sulphophenyl)- 2H-tetrazolium] was used according to the manufacturer's instructions. Bv2 cells, SH-SY5Y cells, and PBMCs were seeded in triplicate in 96-well plates at a density of 1×10^4 cells/well; 24 h post-seeding, cells were treated with different doses of MyVes (0.3, 1.5, and 3 µg/ml) for 72 h. After the treatment, 20 µl of the MTS solution was added to each well and incubated for 4 h at 37°C, 5% CO_2. Absorbance was read at 490 nm using a Glomax microplate reader (Promega). Values are expressed as the percentage of cell growth compared with the control (untreated cells). Treated cultured cells and controls were morphologically analyzed by microscopy using an Axio Scope 2 microscope (Zeiss).

2.7. Analysis of oxidative stress and mitochondrial activity

Mitochondrial membrane potential was measured using a Mito-Probe JC-1 Assay Kit (Molecular Probes, Life Technologies, Invitrogen). Bv2 and SH-SY5Y cells were plated in 96 Well Black/Clear Bottom Plate, for fluorometric measurements, at a concentration of 1×10^5 cells/mL for fluorometric measurements. When the mitochondrial membrane potential has a physiological value, JC-1 can penetrate the mitochondria, forming red fluorescent aggregates. In stressed cells with impaired mitochondrial membrane potential, JC-1 remains outside the mitochondrion and the monomeric form of JC-1 fluoresces green. After the treatment with the different MyVes doses, (0.3, 1.5, and 3 µg/ml dispersion which were pre-filtered with a 0.45 µm sterile filter), the cells were incubated with 2 mM JC-1 (5,50,6,60-tetrachloro-1,10,3,30-tetraethylbenzimidazolyl-carbocyanine iodide) fluorescent dye in PBS (137 mM NaCl, 2.7 mM KCl, 8 mM Na_3PO_4, pH 7.4) for 30 min at 37°C. Carbonyl cyanide 3-chlorophenylhydrazone (CCCp) (50 nM), a potential mitochondrial membrane disruptor, was used as the positive control. By shifting the fluorescence emission of JC-1 from red (590 nm) to green (529 nm), we analyzed the decrease in the red/green fluorescence intensity ratio, which indicates mitochondrial depolarization. Fluorescence was evaluated using a fluorometer (GLOMAX Promega) and fluorescence microscope (Axio Scope 2 microscope; Zeiss) with an excitation laser source at 488 nm.

To evaluate Reactive Oxygen Species (ROS) generation, Bv2 and SH-SY5Y cells were plated in a 96-well black/clear bottom plate at a concentration of 1×10^5/mL1 cells/mL for fluorometric measurements. After treatment with different doses of MyVes (0.3, 1.5, and 3 µg/ml), cells were incubated with 1 µM dichlorofluorescein diacetate (DCFH-DA) in PBS for 10 min at room temperature in the dark. Non-fluorescent DCFH-DA is converted to the highly fluorescent compound, 20,70-dichlorofluorescein (DCF), by cellular esterase activity. DCF emits green fluorescence in the presence of reactive oxygen species (ROS) emits green fluorescence, which is directly proportional to ROS concentration. After washing in PBS, the cells were analyzed using a fluorometer (Glomax Promega) and a fluorescence microscope (Zeiss Axio Scope 2) with excitation at 485 nm and emission at 530 nm.

2.8. Hemolysis assay

For the hemolysis test, 5 ml of blood from healthy human donors was processed according to Picone et al., 2016 [18]. After red blood cells (RBCs) purification, 200 µL of RBCs were pipetted into a 96-well plate. Subsequently, several doses of MyVes (0.3, 1.5, and 3 µg/ml pre-filtered with a 0.45 µm sterile filter) and 10 µL of 10% Triton X-100 (positive control) were added to RBCs. The plates were incubated at 37°C for 2 h. The samples were subjected to morphological analysis by microscopic inspection using an Axio Scope 2 microscope (Zeiss). Subsequently, the plate was centrifuged for 5 min at 500 × g to pellet intact erythrocytes. Next, 100 µL of supernatant was transferred from each well to a clear flat-bottomed 96-well plate. The absorbance of the hemoglobin released following hemolysis in the supernatants was measured using a plate reader at 490 nm (Glomax Promega). After background subtraction, the mean absorbance of the positive control was determined to represent 100% hemolysis. All experimental data were normalized to the absorbance of the positive control.

2.9. MyVes uptake evaluation

For uptake studies, SH-SY5Y and BV2 cells were grown in 96-well plates at a density of 1×10^5 cells/ml and incubated for 2 h with MyVes-Alexa568 or MyVes and unstructured native myelin stained with FluoroMyelin™ Green (3µg/mL dispersions pre-filtered with a 0.45 µm sterile filter). After treatment, cells were fixed in 4% paraformaldehyde in PBS for 30 min at room temperature. After three washes with PBS for nuclear staining, cells were incubated with Hoechst 33258 (5 mg/mL) for 20 min. Image acquisition was performed with an Operetta CLS (Perkin Elmer) using brightfield, DAPI, and Alexa Fluor™ 594 filters and a 40x objective.

2.10. Inflammatory markers of BV2 microglial cells

Cells (1×10^5 cells/mL) were seeded into 24-well plates in the presence or absence of different doses of MyVes (1.5 and 3µg/ml dispersions pre-filtered with a 0.45 µm sterile filter) for 24 h. After treatment, BV2 cells were used to extract total RNA, and RT-PCR was used to analyze the regulation of inflammatory genes. Total RNA was extracted using the High Pure RNA Isolation Kit (Roche) and one µg of RNA was subjected to reverse transcription (RT) using the iScript cDNA Synthesis Kit (Bio-Rad). cDNAs was amplified using the SsoAdvanced Universal SYBER Green Supermix (Bio-Rad) on a StepOne Real-Time instrument (Applied Biosystems). Gene expression was validated using homemade sequence primers for human Interleukin (IL) IL 1β, IL4, IL6, IL10, TNFα, iNOS, and β-actin. Gene expression was normalized to that of β-actin. The comparative quantification method CT ($2^{-\Delta\Delta CT}$) was used to evaluate the relative expression levels of the RNA (StepOne software) (Table 1).

2.11. In-vivo *MyVes biodistribution*

2.11.1. Animals

Thirty-day-old male Wistar rats (≅100 g) were housed three per cage with standard food and water available ad libitum. The animal room had a controlled 12-h light cycle (lights on at 07:00 h), lux level (average 100 lux), temperature (21 ± 1°C), and relative humidity (50 ± 5%). All experiments were conducted in accordance with ARRIVE guidelines. Animal care procedures were con-

Table 1
List of primers.

Gene Name	Gene Symbol	Primer Sequences (F: Forward R: Reverse)
Interleukin 1beta	IL-1β	F: 5′-ATGGCAACTGTTCCTGAACTCAACT-3′ R: 5′-CAGGACAGGTATAGATTCTTTCCTTT-3′
Interleukin 6	IL-6	F: 5′-TCCAGTTGCCTTCTTGGGAC-3′ R: 5′-GTGTAATTAAGCCTCCGACTTG-3′
Tumor necrosis factor alpha	TNF-α	F: 5′-GCCCACGTCGTAGCAAACCAC-3′ R: 5′-GGCTGGCACCACTAGTTGGTTGT-3′
Interleukin 4	IL-4	F:5′-TCCGATTCCTGAAACGGCTC-3′ R:5′-CAACGTACTCTGGCTGGCT-3′
Interleukin 10	IL-10	F:5′-CAGCAGTGCTATGCTGCCTGCT-3′ R:5′-GTGGCTCTGGCCGACTGGGA-3′
Glyceraldehyde-3-phosphate dehydrogenase	GAPDH	F:5′-GCCAAATTCAACGGCACAGT-3′ R:5′-AGATGGTGATGGGCTTCCC-3′

ducted in accordance with the legislation for the protection of animals used for scientific purposes provided by the relevant Italian law and European Union Directive (Italian Legislative Decree 26/2014 and 2010/63/EU) and the International Guiding Principles for Biomedical Research involving animals (Council for the International Organizations of Medical Sciences, Geneva, CH). The animals were subjected to experimental protocols approved by the Veterinary Department of the Italian Ministry of Health (Permit Number: 945/2023-PR). All adequate measures were taken to minimize animal pain or discomfort, and all surgeries were performed under isoflurane anesthesia.

2.11.2 Experimental plan and MyVes intranasal delivery

Fifteen rats were randomly divided into five experimental groups (n=3/group), as follows: healthy rats treated with saline (control), healthy rats treated with unbound Atto 633 solution for 2 or 4 h, and healthy rats treated with MyVes-Atto 633 for 2 or 4 h. The animals were lightly anesthetized with 2% isoflurane in air and the head was elevated to keep the nasal cavity upward. Each rat received two consecutive rounds of 15 µl/nostril of saline, unbound Atto 633 probe or MyVes 633 (total amount 3 mg/kg; stock solution 5 mg/ml dispersion which was pre-filtered with a 0.45 µm sterile filter), using a Hamilton microsyringe and, after the final droplet, the rat's nose was kept pointing upward for 20 s. Two and 4 h post intranasal (i.n.) delivery animals were terminally anaesthetized with ketamine (90 mg/kg) and medetomidine (0.5 mg/kg), and intracardially perfused with 4% (w/v) paraformaldehyde (PFA) in PBS. Brain, lung, liver, heart, spleen, and kidney were dissected and post-perfused overnight in 4% PFA. The organs fluorescence intensity of Atto633 was analyzed using a Typhoon FLA 9500 fluorescence scanner (GE Healthcare Life Sciences) at a resolution of 20 µm (excitation 629 nm and emission 650 nm). The quantification of intensity was performed using the public-domain ImageJ software (US National Institutes of Health, Bethesda, MD), and 3D reconstruction of the fluorescence intensity was performed using ImageMaster 2D Platinum 7.0 - GE Healthcare Life Sciences). Data are reported as the average channel fluorescence of the organs, expressed as relative units after background autofluorescence subtraction (non-injected rat organs).

2.12. Study subjects

Patients with an age range between 18-55 years diagnosed with MS (RRMS according to the McDonald criteria) with an Expanded Disability Status Scale (EDSS) range between 0-5.5 were enrolled. These patients had not received disease-modifying therapies, including glatiramer acetate, IFN-β, and natalizumab, for the past 6 months and had not been taking glucocorticoids for the past 30 days. The study protocol was approved by the Ethics Committee (N 08/2021, September 15, 2021), and informed consent was obtained from all participants. This study was conducted in accordance with the Declaration of Helsinki guidelines.

2.13. Peripheral blood mononuclear cell isolation and measurements of inflammatory markers

Twenty milliliters of venous blood were obtained from each subject. PBMCs will be isolated using the Ficoll-Hypaque isolation technique.[19] To determine cytokine expression 1×10^5 PBMCs/mL for well will be distributed into 24-well plates in the presence or absence of different doses of MyVes (1.5 and 3µg/ml dispersions which were pre-filtered with a 0.45 µm sterile filter) for 72 h. Culture supernatants were collected and stored at - 80C. Interleukin (IL), IL1β, IL10, IL4 and TNFα levels were measured using ELISA (SIGMA).

2.14. Statistical analysis

All experiments were repeated at least three times, and each experiment was performed in triplicates. The results are presented as mean ± SD. One-way ANOVA was performed, followed by Dunnett's post-hoc test for significance analysis. Differences were considered statistically significant at $^{*}p \leq 0.05$, and $^{**}p \leq 0.02$.

3. Results and discussion

3.1. Myelin nanovesicles production and characterization

Myelin was isolated from bovine brain by sucrose fractionation as described in Picone et al, 2021 [15]. With respect to the data reported in Picone et al. 2021 [15], myelin was extracted from bovine brain for the biofabrication of nanovesicles (Fig. 1A). The bovine brain was significantly larger than the rat brain. This not only provides a larger amount of starting material, but also allows the selection of white matter rich in myelin fibres for the extraction of purer myelin. Myelin has a water content of about 40% and the dry mass of myelin is characterized by a high proportion of lipids (70 to 85%) and consequently a low proportion of proteins (15 to 30%). In contrast, most biological membranes have a higher protein/lipid ratio. Analysis of the composition of bovine and human myelin shows remarkable similarity, in line with findings in various mammalian species [20]. However, there are some species differences; for example, rat myelin contains less sphingomyelin than bovine or human myelin [20]. Moreover, the bovine myelin has been administered orally to MS patients [16].

MyVes were obtained by nanoprecipitation of a myelin solution according to a previously reported procedure [15] (Fig. 1A). Briefly, dripping of the solutions of myelin extracts in water was performed by mixing with Ultraturrax®(U). To confirm the nature of the nanovesicle, MyVes were stained with FluoroMyelin™

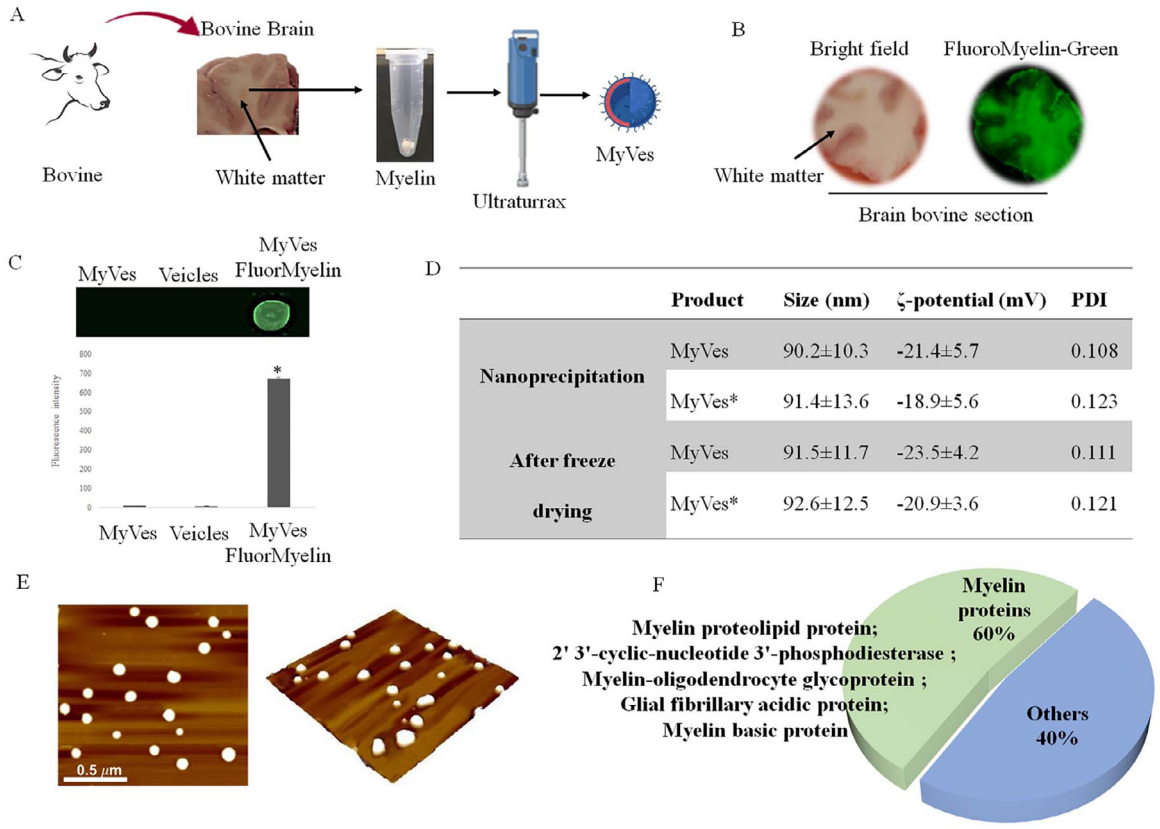

	Product	Size (nm)	ζ-potential (mV)	PDI
Nanoprecipitation	MyVes	90.2±10.3	-21.4±5.7	0.108
	MyVes*	91.4±13.6	-18.9±5.6	0.123
After freeze drying	MyVes	91.5±11.7	-23.5±4.2	0.111
	MyVes*	92.6±12.5	-20.9±3.6	0.121

Fig. 1. Bio-fabrication of myelin nanovesicles. (A) Schematic representation of myelin extraction from bovine brain tissue, freeze-dried myelin in a vial, and nanoprecipitation by ultraturrax to generate MyVes. (B) Myelin staining in bovine brain cryosections by FluoroMyelin™ Green and (C) image by fluorescence scanner and relative histogram of the fluorescence levels of MyVes staining using FluoroMyelin™ Green. (D) Table of physical characteristics of MyVes: size, ζ potential, and PDI values after production by nanoprecipitation and after freeze-drying. (E) 2D and 3D AFM images of MyVes (F) Pie chart of MyVes proteins identified by RP-nUHPLC/nESI-MS/MS and subsequently database search. *p≤ 0.05, FluoroMyelin *vs* MyVes.

Green, which allows rapid and selective labeling of myelin in brain cryosections (Fig. 1B). As shown in Fig. 1C, MyVes exhibited high green fluorescence, which confirmed their high myelin content. The Size, Z potential, and polydispersity index (PDI) values of MyVes and MyVes labeled with a fluorescent probe (MyVes*) were measured using Dynamic Light Scattering (DLS). Dialysis diffusion test performed on labeled MyVes did not showed quantifiable amount of dye leaching over 3 days of thus suggesting stability of linkage occurred between MyVes and Atto 633. The nanoprecipitation of a myelin solution by solvent injection technique generates nanoparticles with a size of about 90.2 nm for MyVes, and 91.4 nm for MyVes* (Fig. 1D-Table). After the redispersion of freeze-dried products were obtained vesicles with a size of 91.5 nm for MyVes, and 92.6 nm for MyVes*. To evaluate the stability of myelin nanovesicles in solution, ζ-potential values were measured. The ζ-potential values, reported in Fig. 1D-Table, ranging from -18 to -23 mV. Moreover, size dimensional distribution of MyVes was followed also at 37°C for 48 h after redispersion of freeze-dried sample in DMEM at pH 7.4. As reported in Table S1 of supplementary, in such conditions MyVes maintained a mean size of 90 nm throughout the experiment. The dimensional range of MyVes was confirmed also by atomic force microscopy (AFM). 3D and 2D AFM images are reported in Fig. 1E. These results demonstrate that by employing nanoprecipitation, it is possible to produce nano-sized vesicles with high stability in water. Furthermore, freeze-drying had no impact on vesicle stability. To characterize the proteomic composition of MyVes, an in-solution digestion protocol was performed after a purification step to remove all non-protein contaminating molecules. The peptide mixture was analyzed in triplicate using reversed-phase nano-ultra-high-performance liquid chromatography-nano-electrospray ionization-tandem mass spectrometry (RP-nUHPLC/nESI-MS/MS). Subsequently, the mass spectrometric data were searched against the SwissProt database, which is restricted to Bos taurus taxonomy. In agreement with the data reported in the literature, approximately 60% of these identifications are the main known myelin proteins, such as Myelin Basic Protein (MBP), myelin Proteolipid Protein (PLP), 20-30-Cyclic-Nucleotide 30-Phosphodiesterase protein (CNP), Myelin-Associated Glycoprotein (MAG), calmodulin-1, and Myelin-Oligodendrocyte Glycoprotein (MOG) (Fig. 2F) [15,19,20].

3.2. Myelin nanovesicles cytocompatibility and hemocompatibility

Biocompatibility is one of the key requirements for assessing the quality of biomaterials used in clinical applications. The first step in assessing biocompatibility is a cytotoxicity test in which cultured cells are directly exposed to the test material. To test the safety of MyVes, we performed different assays by treating the cells with different MyVes concentrations (0.3, 1.5, and 3 μg/ml) for 72 h. As shown in Fig. 2A, where MTS viability data are reported, MyVes did not induce cytotoxicity in neuronal (SH-SY5Y) and microglial (BV2) cells at any of the doses tested, confirming the cytocompatibility of MyVes. The results of the MTS viability assay (Fig. 2A) were analyzed according to the ISO10993-5 standard guidelines, where a biomaterial was considered cytotoxic when cell viability was below 70% [21]. Cytocompatibility was confirmed by microscopic inspection, where no morphological changes were observed in any of the treated cell lines (Fig. 2B). Furthermore, no

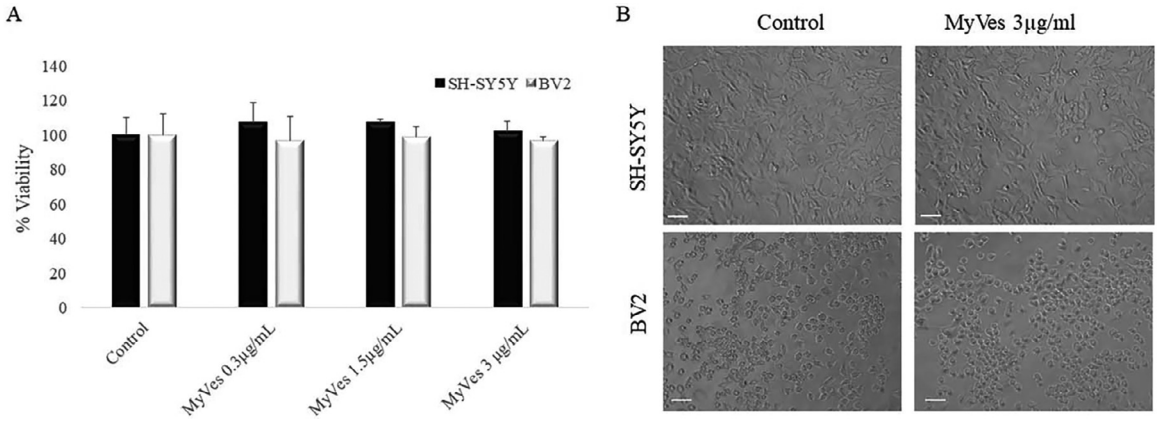

Fig. 2. MyVes Cytocompatibility. Cell viability (A) and morphological analysis (B) of microglia (BV2) and neurons (SH-SY5Y) treated for 48 h with MyVes at different doses. White bar represents 50µm.

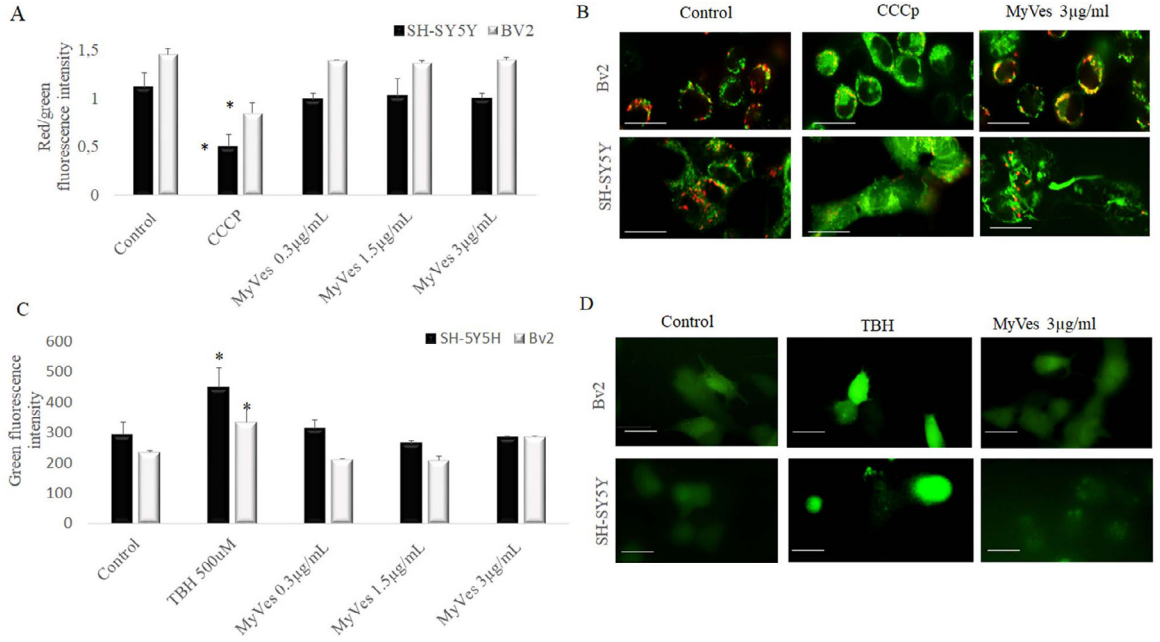

Fig. 3. Mitochondrial and oxidative stress analysis. a Histogram relative to the JC-1 red/green fluorescence ratio of neurons and microglial cells untreated (control) or treated with MyVes at different concentrations for 24 h or with CCCp (positive control). b Fluorescence microscopy images of the JC-1 test of MyVes at the highest dose (3µg/ml) compared to control cells and CCCp treated cells; merged image of green and red fluorescence is shown. c Histogram showing the green fluorescence intensity recorded in DCF assay for untreated (control) or treated neurons and microglial cells with MyVes at different concentrations or TBH treated cells (positive control) for 24 h. d Fluorescence microscopy images of the DCF test of MyVes at the highest dose compared to control cells and TBH treated cells. *$p \leq 0.05$, treated vs control groups. White bar represents 20µm.

proliferative effects were observed at any of the concentrations tested (Fig. 2A).

Other parameters commonly used as indicators of cell health are mitochondrial membrane potential and oxidative stress. SH-SY5Y and BV2 cells were treated with MyVes for 24 h and a JC-1 assay was performed, in which mitochondrial membrane depolarization was observed as a decrease in the red/green fluorescence intensity ratio. In samples treated with MyVes, the red/green fluorescence was comparable to that of untreated cells (control), indicating that the physiological mitochondrial membrane potential was not altered (Fig. 3A). Conversely, the red/green fluorescence decreased in the CCCp sample (positive control) (Fig. 3A). Red and green fluorescence was also visualized using confocal microscopy (Fig. 3B). To analyze the effect of MyVes on oxidative stress, the DCFH-DA assay was used to detect intracellular reactive oxygen species (ROS) according to the ISO10993-5 standard guidelines [21]. Fluorometric analysis and fluorescence microscopy showed that the presence of intracellular ROS in MyVes-treated samples was comparable to basal (control) levels (Fig. 3C, D). In contrast, increased fluorescence was observed in tert-butylhydroperoxide (TBH) treated sample used as positive control (Fig. 3C, D). These results unequivocally demonstrated that MyVes did not induce cellular death, proliferative processes, or activated mitochondrial or oxidative stress. All parameters analyzed were maintained at basal levels.

Although there are various routes of administration, including subcutaneous, intramuscular, intravenous, intraperitoneal and intranasal, a phenomenon of absorption of the drug into the bloodstream has been found in all of them. For example, although intranasal administration offers a non-invasive approach to directly access the CNS via the olfactory or trigeminal systems, it is critical to consider absorption into the bloodstream, lymphatic system and cerebrospinal fluid [22]. Consequently, the design of nanomaterials for medical applications must prioritize hemocompatibil-

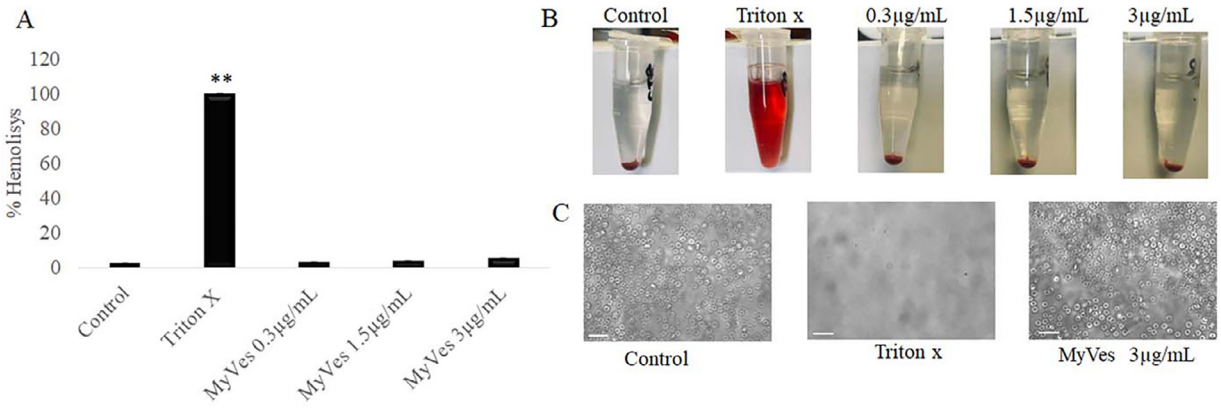

Fig. 4. MyVes Hemocompatibility. (A) Histogram showing the percentage of hemolysis, spectrophotometrically measured, of untreated erythrocytes (Control) or treated with Triton-X100 (positive control) or with MyVes at different concentrations, for 4 h. (B) Photographs of the tubes of human erythrocytes untreated, incubated with Triton-X100 and with different MyVes concentration after centrifugation. (C) Microscopic images of untreated erythrocytes (Control) or treated with Triton-X100 and with MyVes at the highest dose. **p≤ 0.02, Triton-X vs control group. White bar represents 20µm.

ity, particularly where interaction with blood cells is expected, to mitigate any potential side effects or adverse reactions. We evaluated the integrity of red blood cells, considered an index of hemocompatibility, in the presence of MyVes by measuring the release of hemoglobin, as suggested by the ISO 10993-4 standard guidelines. Erythrocytes were incubated with or without MyVes, and the amount of free plasma hemoglobin (Hb) was measured as a hemolytic index using a spectrophotometer. As shown in Fig. 4A, complete hemolysis was observed in samples treated with Triton-X, which was used as a positive control, whereas MyVes-induced hemolysis was similar to that of the untreated sample (Control) (Fig. 4A, B). These results were supported by microscopic analysis of the erythrocytes, where the morphology of the MyVes-treated erythrocytes was similar to that of the control (Fig. 4C).

Moreover, to evaluate whether MyVes could produce injurious effects on blood cells, we treated Peripheral Blood Mononuclear Cells (PBMCs) extracted from healthy volunteers with MyVes at different concentrations and lipopolysaccharide (LPS), an activator of the inflammatory response (positive control). The viability of treated PBMCs was comparable to that of untreated cells (control) at all the concentrations tested (Fig. 5A). In contrast, LPS treatment induced proliferation as an immunostimulatory effect (Fig. 5A) [18]. Accordingly, morphological evaluation of PBMCs (Fig. 5B) showed the typical activation clusters induced by LPS treatment; whereas no differences were observed between untreated and MyVes-treated PMBCs. To confirm these data, the production of interleukin 1β was also evaluated. As shown in Fig. 5C, treatment with different doses of MyVes did not result in an increase in this interleukin; however, LPS, used as a positive stimulus for the inflammatory process, produced a significant increase in IL1β. In conclusion, the MyVes system fulfils all the preliminary requirements for use as a nanosystem in medical applications, being non-cytotoxic, non-immunogenic and hemocompatibile.

3.3. MyVes microglia cell uptake and anti-inflammatory effect

Previous results indicated that MyVes, obtained from mouse myelin, have a preferential ability to target microglial cells [15]. This effect agrees with the literature, in fact microglia are the key effector cells that clear myelin debris [23]. Several receptors are involved in the process of receptor-mediated myelin phagocytosis in microglial cells, including complement receptor 3 (CR3), scavenger receptors (SR-AI/II and collective placenta 1 (CL-P1)), Fc receptors, CD36, MerTK. and trigger receptor expressed on myeloid cells-2 (TREM2). Other receptors, such as low-density lipoprotein receptor-related protein 1 (LRP1) and a scavenger receptor called macrophage receptor with a collagenous structure (MARCO), may also serve as receptors for myelin in macrophages [24]. To confirm that MyVes produced from bovine brain have this potential, we performed an *in vitro* experiment using neurons and microglial cells. To test the uptake and follow the fate of MyVes, it was possible to label MyVes proteins with the succinimidyl ester Alexa Fluor 568 (MyVes-Alexa 568) (Fig. 6A). After confirming the high fluorescence of MyVes-Alexa 568 (Fig. 6B), the MyVes were incubated in neurons and microglia for 4 h. Fluorescence microscopy images (Fig. 6C) showed that the highest levels of fluorescence were detected in the microglial (BV2) cells.

Microglia are the resident innate immune cells of the CNS that play an important role in the inflammatory and immune response in MS [8]. Active microglia can be divided into M1 and M2 subgroups. M1 microglia promote the production of inflammatory cytokines such as IL-1β, IL12, IL6, IL8, and TNFα, nitric oxide (NO) and Reactive Oxygen Species (ROS) production. M2 microglia secrete anti-inflammatory cytokines, such as IL-10, IL4, CD206 (mannose receptor), CCL22, and Arg1 (arginase) [23,25]. To study the effect of MyVes on microglia, cells derived from raf/myc-immortalised murine neonatal microglia (BV-2), the same cells used for the uptake studies were used. This cell line is the most frequently used substitute for primary microglia, and has been widely used for pharmacological studies, studies of phagocytosis, and for many important immunological discoveries [26]. Several studies have shown that myelin phagocytosis by microglia and macrophages can enhance neuroinflammation [27–29]. In contrast, other studies have reported an anti-inflammatory effect of microglia upon myelin phagocytosis [25,30]. Our system differs from those of previous studies. Nanostructuring of myelin leads to the production of nanovesicles that can acquire biological properties different from those of non-nanostructured myelin. The physicochemical properties of nanostructures, such as their size, surface chemistry, surface charge, and shape, are important factors that influence binding, uptake, and biological responses. To address this issue and to understand the biological response of MyVes, we treated BV2 cells with different concentrations of MyVes. The results shown in Fig. 7A–C indicate that MyVes did not induce an increase in inflammatory cytokines (IL-1β, IL-6, TNF-α) and, importantly, induced an increase in IL-4 (Fig. 7D). Furthermore, we demonstrated an increased uptake of MyVes in microglia cells compared to non-nanostructured myelin (Fig. S1) and an absence of IL4 expression after treatment with non-nanostructured myelin (Fig. S2).

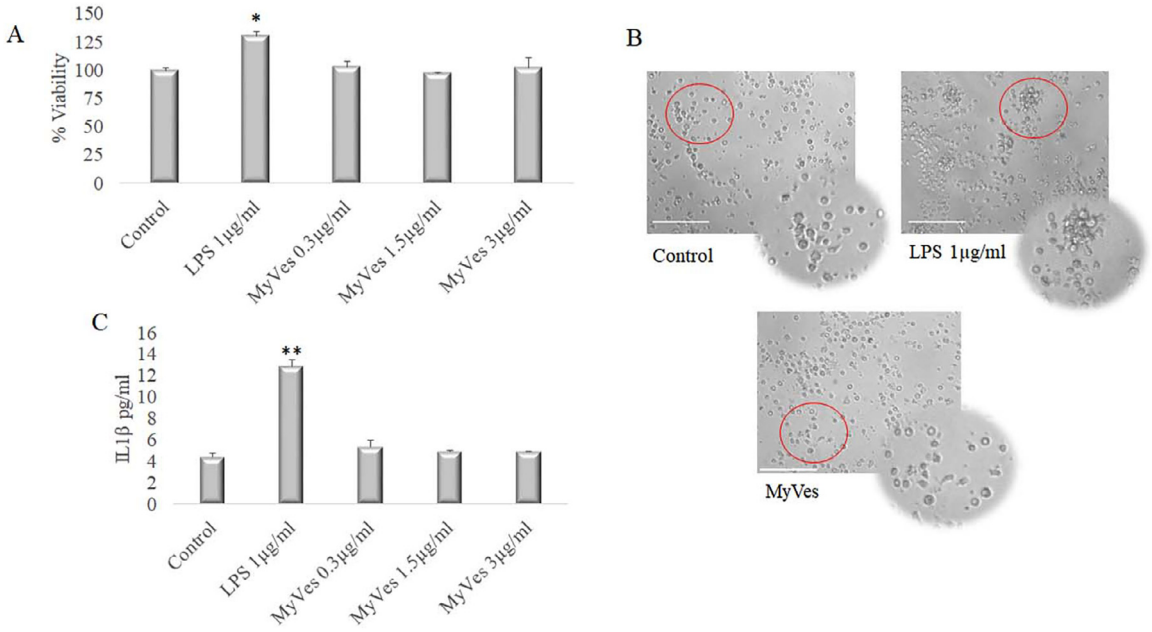

Fig. 5. Immunocompatibility of MyVes (A) Histogram of viability of PBMCs untreated (Control) or treated with LPS or different concentrations of MyVes. *p≤ 0.05, LPS treated vs control group. (B) Morphological evaluation of PBMCs. No differences were detected between untreated and MyVes treated cells, while the clusters activation after LPS treatment was observed. (C) ELISA quantification of Interleukin 1β levels in supernatants of untreated PBMCs (Control), treated with MyVes at different concentrations and LPS. **p≤ 0.02, LPS treated vs control group. White bar represents 20µm.

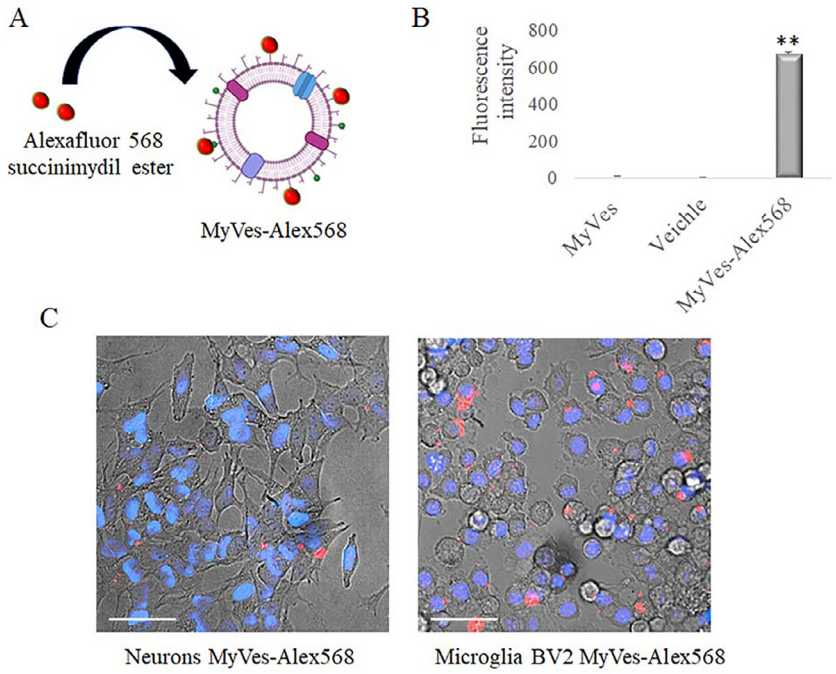

Fig. 6. Interaction of MyVes with microglial cells *in vitro*. (A) Schematic representation of the MyVes labeled with succinimidyl ester Alexa Fluor 568 (MyVes-Alexa 568) and (B) relative histogram of the fluorescence intensity levels of MyVes-Alex 568. **p≤ 0.02, MyVes-Alexa 568 vs control group. (C) representative fluorescence images of neurons (SH-SY5Y) and microglia (BV2) cells incubated with MyVes-Alexa 568 for 2 h. White bar represents 50µm.

IL-4 is a pleiotropic cytokine that regulates brain homeostasis, supports oligodendrogenesis and neurogenesis, and is a potent regulator of immunity [31]. IL-4 is neuroprotective in animal models of MS, cerebral ischemia, spinal cord injury and amyotrophic lateral sclerosis (ALS) [32–34]. Studies on the severity of EAE (Experimental Autoimmune Encephalomyelitis, MS animal model) in IL-4−/− mice compared to wild-type mice suggest a potential protective role of IL-4 against the incidence and progression of MS [35]. Liu et al. demonstrated that the mechanism leading to the down-regulation of microglial inflammation following myelin phagocytosis is due to the generation of ROS via p47-PHOX [25].

3.4. Pharmacokinetics of MyVes intranasally delivered to the brain

To investigate the ability of MyVes to reach the brain and their possible pharmacokinetics after intranasal (i.n.) delivery, we treated healthy animals with labeled MyVes via the i.n. route and analyzed the dissected organs two and four hours after treatment.

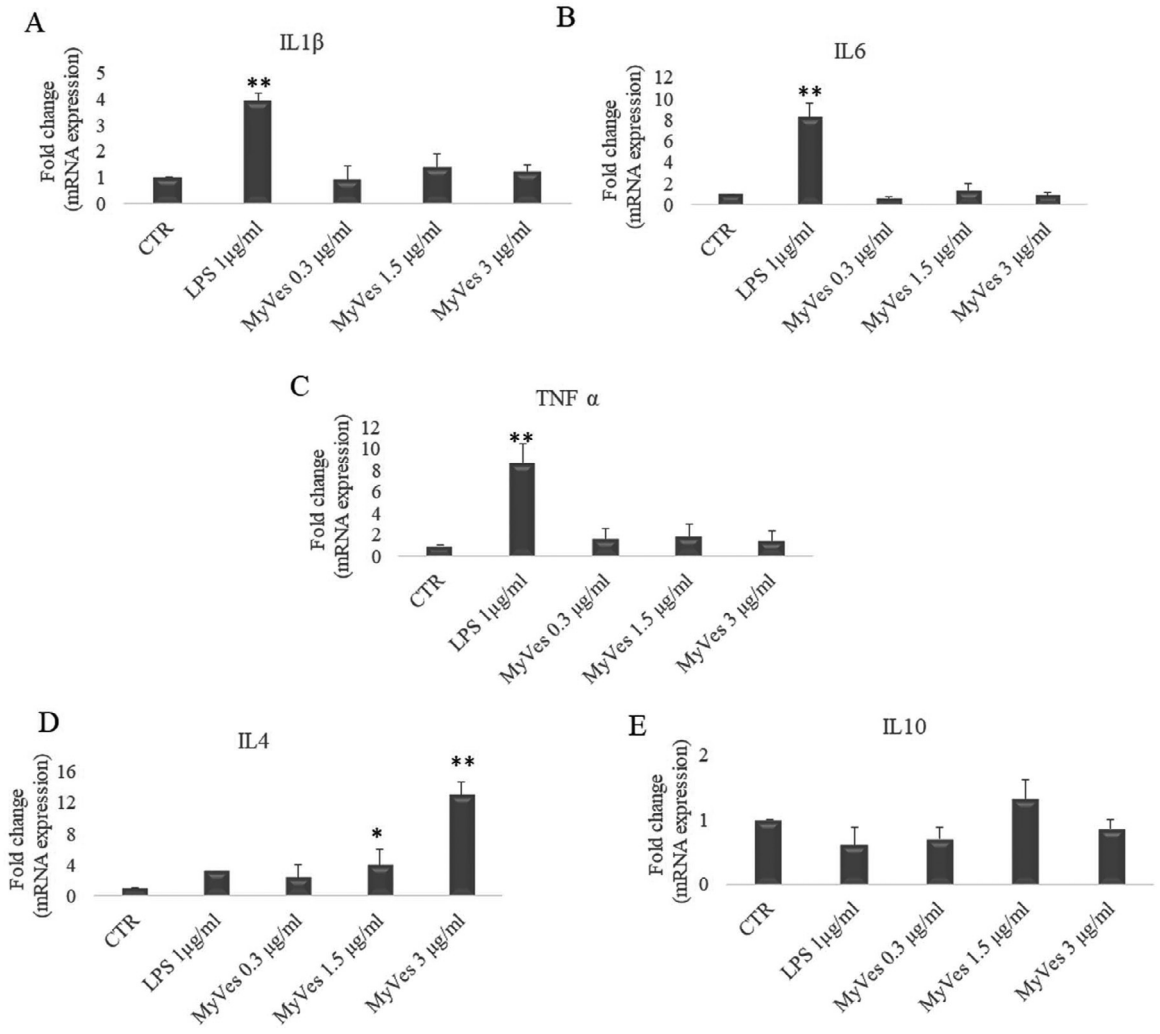

Fig. 7. MyVes induces the expression of the anti-inflammatory cytokine IL 4 in microglial cells. The mRNA expression of IL-1β (A), IL-6 (B), TNF-α (C), IL-4 (D) and IL-10 (E) was evaluated by real-time PCR. $^{*}p \leq 0.05$, and $^{**}p \leq 0.02$, treated vs control groups.

We chose to study i.n. administration for brain drug delivery because the common routes of administration, such as oral and intravenous, have limitations in releasing the drug into the brain, such as the presence of the blood-brain barrier (BBB), the large effect of the first metabolic step, and the dispersion of the drug in the body. Therefore, non-invasive i.n. delivery of biomolecules to bypass the BBB and reach the brain parenchyma could be an alternative and is currently attracting attention as an effective route for drug delivery to the brain. The graphic sketch in Fig. 8 schematizes the procedure used for the analysis of the cerebral distribution of MyVes after i.n. treatment (Fig. 8A) and shows the outcome of the MyVes labeling procedure using the Atto 633 fluorescent probe (Fig. 8B). Scanner fluorescence measurements of whole brains (Fig. 8C and D) showed that MyVes reached the brain after i.n. administration and localized preferentially in the olfactory bulbs, cerebellum and brainstem nuclei (Fig. 8D). The fluorescence intensity, measured for the whole brain, peaked 2 h after treatment and then decreased. However, it remained significantly different from that observed in saline-treated rats and unbound Atto 633 probe-treated animals 4 h after treatment (Fig. 8E).

Fluorescence analysis was performed on brain axial cross sections to confirm the distribution of MyVes in the brain. Specifically, 2 mm thick brain slices were cut coronally in the anteroposterior direction (Fig. 9A) and then analyzed using a fluorescence scanner (Fig. 8B) and 3D reconstruction (Fig. 9C). Two hours after i.n. treatment, the fluorescence intensity of the labeled MyVes was localized in the olfactory bulbs and cerebellum, as confirmed by the analyses of the fluorescence on the sagittal plane (Fig. 9D). The biodistribution study of MyVes in the major organs of the mouse showed that MyVes not only accumulated in the brain, but also localized in the liver and kidneys (Fig. S3), which are critical for the body's excretory processes. Furthermore, 4 h after administration, fluorescence is reduced in the organs analyzed (Fig. S3), indicating that MyVes has probably been cleared from the body. These data are in agreement with the literature where *ex vivo* studies on the biodistribution of brain fluorescence of different nanosystems have shown that after intranasal administration, the fluorescent signal was detected in the brain between 1 and 3 h and was eliminated via the liver and kidneys [36,37].

Based on these biodistribution experiments, we hypothesized that the passage of MyVes from the nose to the brain may allow targeting of the olfactory bulbs and mediate the reaching of the posterior areas of the brain via the trigeminal nerve. The spinal cord begins at the base of the brain and is frequently affected in MS. Several pathological abnormalities, including demyelination and neuroaxonal loss, occur in the spinal cord in MS, causing motor, sensory and autonomic dysfunction, and have been studied *in vivo* using magnetic resonance imaging (MRI). MyVes, which

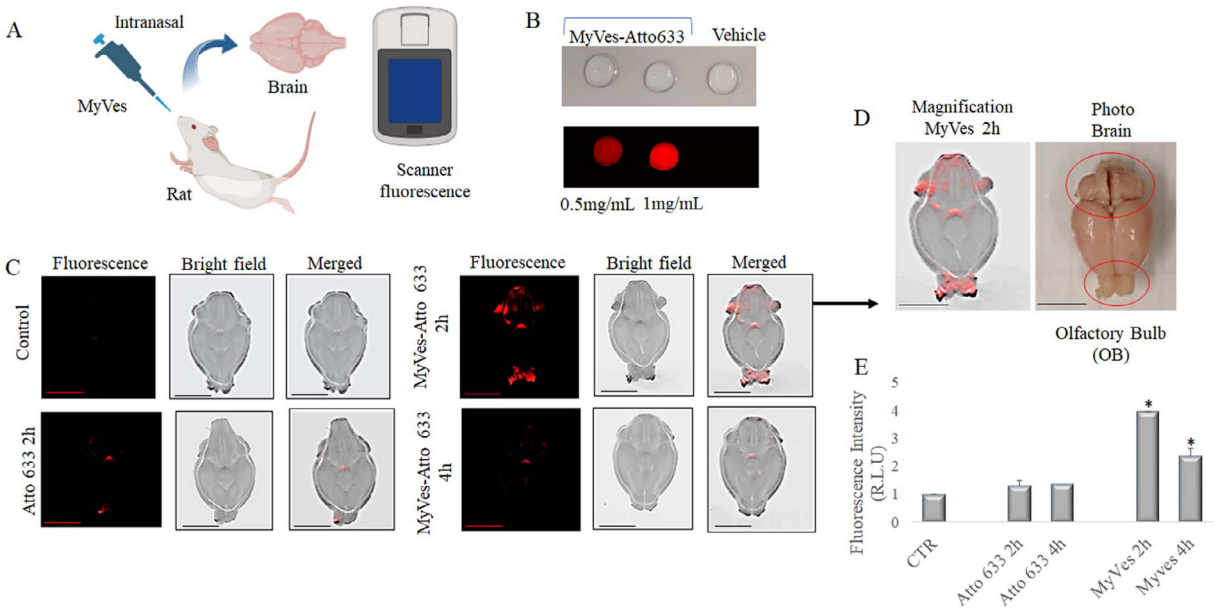

Fig. 8. *Ex vivo* fluorescence images of brain biodistribution of the MyVes in rats. (A) Scheme of procedure used for intranasal treatment and MyVes brain distribution analysis. (B) Fluorescence scanner image of the intensity of the vehicle (PBS), and 0.5mg/ml and 1mg/ml NyVes-Atto633. (C) Representative brain fluorescence images of the labeled MyVes at 2 and 4 h post intranasal injection. (D) High-magnification images of the brain s are highlighted in the square. (E) Histogram related to brain fluorescence quantification analysis. *p ≤ 0.05 treated vs control groups. Black and red bar represents 1 cm.

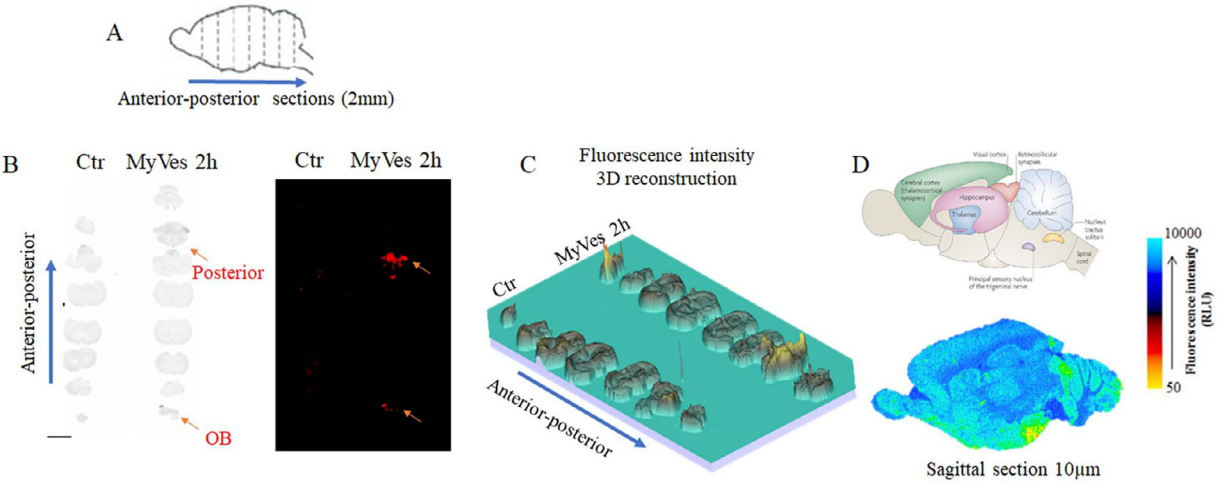

Fig. 9. *Ex-vivo* fluorescence images of MyVes brain biodistribution. (A) Representative scheme and (B) fluorescence images of 2 mm thick-coronal sections of control and 2 h post-i.n. MyVes rats, black bar represents 1 cm. (C) 3D reconstruction of the fluorescence intensity values. (D) Fluorescence images of 10µm sagittal sections at 2 h post MyVes i.n, administration.

reaches the most posterior part of the brain closest to the spinal cord, could reach the sites of demyelination typical of MS. Further preclinical experiments in control and MS-affected rats will be required to investigate the therapeutic efficacy of intranasally administered MyVes in ameliorating the myelin changes and neuromotor dysfunction characteristic of MS, exploiting the enhanced white matter tropism of MyVes [15].

3.5. MyVes immunomodulatory effect on PBMCs from multiple sclerosis patients

MS is an inflammatory disease characterized by infiltration of peripheral mononuclear lymphocytes into the CNS. Specifically, activated B and T lymphocytes leave lymphoid tissues and migrate across the BBB into the CNS, and upon re-encountering myelin antigens, they damage the myelin sheath [38,39]. Several studies have used Peripheral Blood Mononuclear Cells (PBMCs) from the blood of MS patients as a model to test the immunomodulatory effects of different drugs and drug delivery systems [40–45]. The dysregulation of Th1 and Th2 cytokines in MS is well established [40]. Studies have demonstrated that the Th1 subset of CD4+ T cell cytokines (proinflammatory IL-1β, TNFα,) is increased during disease activity, whereas Th2 cytokines (anti-inflammatory IL-4, IL-10) are increased during reduced disease activity [45,46].

To determine whether MyVes could shift the balance towards either Th1 or Th2, we measured the cytokines released by PBMCs isolated from MS patients treated with different doses of MyVes. A summary of the clinical data of the enrolled MS patients who underwent PBMC collection is shown in Fig. 10A. After MyVes treatment, PBMCs supernatants were collected, and the levels of IL-1β, TNFα, IL-4 and IL-10, were measured by ELISA (Fig. 10B). These results indicated that MyVes did not induce significant activation of

A

Patient ID	Sex	Age	MS subtype	Duration	EDDS
MS1	F	36	RRMS	16	4.5
MS2	F	54	RRMS	9	5.5
MS3	F	58	RRMS	5	5.5
MS4	F	59	RRMS	9	5.5
MS5	M	69	RRMS	19	4.5
MS6	M	70	RRMS	30	6.0

B

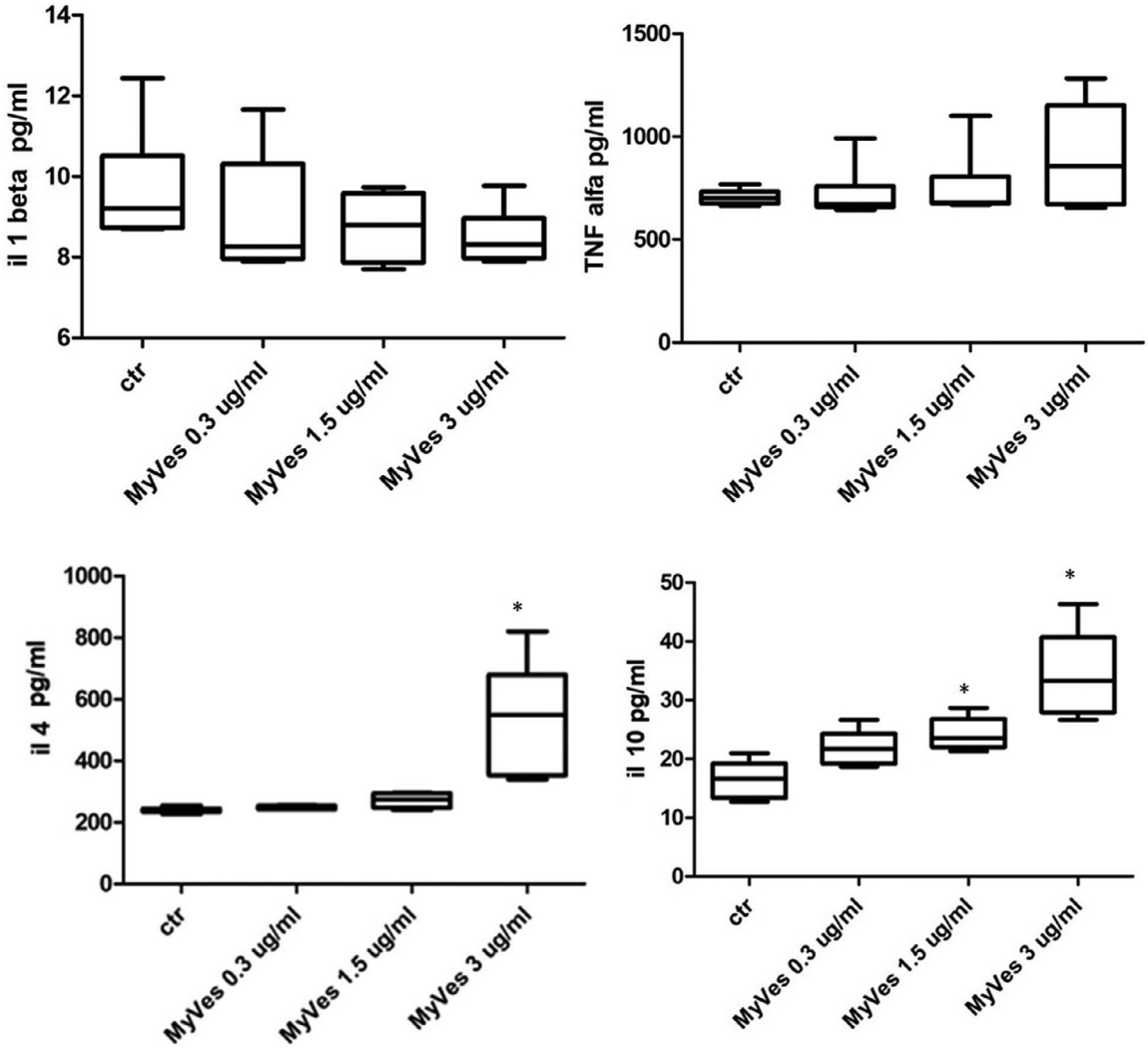

Fig. 10. MyVes Immunomodulatory effect on PBMCs from MS patients (A) Demographic and clinical data of the cohort selected. F, female; M, male; RRMS relapsing-remitting multiple sclerosis, EDDS, Expanded Disability Status Scale. (C) Levels of IL-1β, TNF-α, IL-4 and IL-10 using IL-specific ELISA kits. *p $\leq$ 0.05 treated vs control groups.

the pro-inflammatory cytokines IL 1β and TNFα; however, it is interesting to note that they increased the production of IL-10 and IL-4.

Induction and/or administration of the anti-inflammatory cytokines IL-10 and IL-4 can significantly contribute to the amelioration of the first attack of the disease in MS patients [47].

We hypothesized that since MyVes naturally contain myelin proteins, a realistic scenario would be that antigen presenting cells (APCs) present in PBMCs internalize MyVes by presenting these peptides to other immune cells, thereby inducing an immunomodulatory effect. Several parameters can influence nanoparticle interactions, including nanoparticle size, shape, surface and charge. Nanomaterials ranging from a few nanometers to more than a micrometer have been documented to be successfully and completely internalized by dendritic cells (DCs) [48,49]. In addition, DCs may be able to discriminate nanoparticles based on their shape; for

example, rod-shaped nanoparticles elicit a pro-inflammatory response. The surface chemistry of the nanoparticle provides properties such as hydrophilicity and charge, which can either facilitate or hinder the uptake and response of DCs. Highly charged nanoparticles (positively or negatively charged) have been colloidally stabilized by electrostatic repulsion. Furthermore, studies have shown that cationic nanoparticles are more likely to be internalized by cells, including DCs [50], but can also be highly immunogenic [51]. On the other hand, negatively charged particles have been reported to reduce acute inflammation in immune disorders [52]. Thanks to their characteristics, such as: size, shape, surface, and charge, the MyVes could be easily internalized by APC cells. It is now generally accepted that myelin-derived proteins are the major antigens targeted by autoreactive responses in MS [1]. However, the wide variety of myelin-derived antigens associated with MS poses challenges for the selection of target antigens for antigen-specific therapies. MyVes that simultaneously transport all the major antigens targeted by autoreactive responses in MS, together with their physicochemical properties (size, shape, charge), are suitable for nanomedicine and have great potential to induce antigen-specific tolerance in MS.

4. Conclusion

In this study, we extracted myelin from bovine brain tissue and produced MyVes by nanoprecipitation. MyVes have an average diameter of approximately 100 nm, negative zeta potential, contain the major myelin sheath proteins, and are cytocompatible and hemocompatible. In addition, the biodistribution profile of MyVes after intranasal administration suggests their ability to reach the brain, and *in vitro* experiments indicate that MyVes can target microglial cells by modulating the anti-inflammatory phenotype. Finally, in peripheral blood mononuclear cells (PBMCs) isolated from multiple sclerosis (MS) patients, MyVes administration induced the production of the anti-inflammatory cytokines IL-10 and IL-4. The data provide an initial proof-of-concept demonstration of the potential of MyVes against MS. However, further preclinical studies are required to confirm fate of vesicles during diffusion from nose to brain and clinical potential.

Funding

This research was supported by EU funding within the MUR PNRR "National Center for Gene Therapy and Drugs based on RNA Technology" (Project no. CN00000041 CN3 RNA).

Declaration of competing interest

The authors declare that they have no known competing financial interests or personal relationships that could have appeared to influence the work reported in this paper.

CRediT authorship contribution statement

Pasquale Picone: Writing – review & editing, Writing – original draft, Supervision, Methodology, Funding acquisition, Formal analysis, Conceptualization. **Fabio Salvatore Palumbo:** Writing – review & editing, Writing – original draft, Supervision, Methodology, Funding acquisition, Formal analysis, Conceptualization. **Francesco Cancilla:** Methodology, Formal analysis, Conceptualization. **Antonella Girgenti:** Methodology, Formal analysis, Conceptualization. **Patrizia Cancemi:** Supervision, Methodology, Conceptualization. **Vera Muccilli:** Software, Methodology, Conceptualization. **Antonella Di Francesco:** Methodology, Formal analysis. **Maura Cimino:** Formal analysis, Data curation. **Chiara Cipollina:** Methodology, Data curation, Conceptualization. **Marzia Soligo:** Investigation, Formal analysis, Conceptualization. **Luigi Manni:** Methodology, Formal analysis, Conceptualization. **Gianluca Sferrazza:** Methodology, Formal analysis, Conceptualization. **Luca Scalisi:** Methodology, Formal analysis. **Domenico Nuzzo:** Writing – review & editing, Writing – original draft, Supervision, Methodology, Formal analysis, Conceptualization.

Acknowledgments

This research was supported by EU funding within the MUR PNRR "National Center for Gene Therapy and Drugs based on RNA Technology" (Project No. CN00000041 CN3 RNA).

Supplementary materials

Supplementary material associated with this article can be found, in the online version, at doi:10.1016/j.actbio.2024.08.016.

References

[1] M.P. Amato, G. Ponziani, M.L. Bartolozzi, G. Siracusa, A prospective study on the natural history of multiple sclerosis: clues to the conduct and interpretation of clinical trials, J. Neurol. Sci. 15 (1999) 96–106.
[2] C. Baeche-Allan, B.J. Kaskow, H.L. Weiner, Multiple sclerosis: mechanisms and immunotherapy, Neuron 97 (2018) 742–768.
[3] M.S. Weber, B. Hemmer, Cooperation of B cells and T cells in the pathogenesis of multiple sclerosis, Results Probl. Cell Differ. 51 (2010) 115–126.
[4] J.M. Goverman, Immune tolerance in multiple sclerosis, Immunol. Rev. 241 (2011) 228–240.
[5] O. Kammona, C. Kiparissides, Recent advances in antigen-specific immunotherapies for the treatment of multiple sclerosis, Brain Sci. 29 (2020) 333.
[6] A. Lutterotti, H. Hayward-Koennecke, M. Sospedra, R. Martin, Antigen-specific immune tolerance in multiple sclerosis-promising approaches and how to bring them to patients, Front. Immunol. 22 (2021) 640935.
[7] P.S. Giacomini, A. Bar-Or, Antigen-specific therapies in multiple sclerosis, Expert Opin. Emerg. Drugs 14 (2009) 551–560.
[8] C. Luo, C. Jian, Y. Liao, Q. Huang, Y. Wu, X. Liu, D. Zou, Y. Wu, The role of microglia in multiple sclerosis, Neuropsychiatr. Dis. Treat. 26 (2017) 1661–1667.
[9] M.P. Mycko, R. Papoian, U. Boschert, C.S. Raine, K.W. Selmaj, cDNA microarray analysis in multiple sclerosis lesions: detection of genes associated with disease activity, Brain 126 (2003) 1048–1057.
[10] A.J. Thompson, S.E. Baranzini, J. Geurts, B. Hemmer, O. Ciccarelli, Multiple sclerosis, Lancet 391 (2018) 1622–1636.
[11] D. Nuzzo, P. Picone, Multiple sclerosis: focus on extracellular and artificial vesicles, nanoparticles as potential therapeutic approaches, Int. J. Mol. Sci. 122 (2021) 8866.
[12] P. Picone, D. Nuzzo, Biofabrication of nanovesicles for brain diseases, Neural Regen. Res. 18 (2023) 525–526.
[13] P. Picone, G. Porcelli, C.C. Bavisotto, D. Nuzzo, G. Galizzi, P.L. San Biagio, D. Bulone, M. Di Carlo, Synaptosomes: new vesicles for neuronal mitochondrial transplantation, J. Nanobiotechnol. 6 (2021) 19(1):6.
[14] P. Picone, D. Nuzzo, Promising treatment for multiple sclerosis: mitochondrial transplantation, Int. J. Mol. Sci. 17 (4) (2022) 2245 23.
[15] P. Picone, F.S. Palumbo, S. Federico, G. Pitarresi, G. Adamo, A. Bongiovanni, A. Chaves, P. Cancemi, V. Muccilli, V. Giglio, V. Vetri, S. Anselmo, G. Sancataldo, V. Di Liberto, D. Nuzzo, Nano-structured myelin: new nanovesicles for targeted delivery to white matter and microglia, from brain-to-brain, Mater. Today Bio 7 (2021) 100146.
[16] H.L. Weiner, G.A. Mackin, M. Matsui, E.J. Orav, S.J. Khoury, D.M. Dawson, D.A. Hafler, Double-blind pilot trial of oral tolerization with myelin antigens in multiple sclerosis, Science 26 (1993) 1321–1324.
[17] A. Cucina, V. Cunsolo, A. Di Francesco, R. Saletti, G. Zilberstein, S. Zilberstein, A. Tikhonov, A.G. Bublichenko, P.G. Righetti, S. Foti, Meta-proteomic analysis of the Shandrin mammoth by EVA technology and high-resolution mass spectrometry: what is its gut microbiota telling us? Amino Acids 53 (2021) 1507–1521.
[18] P. Picone, L.A. Ditta, M.A. Sabatino, V. Militello, P.L. San Biagio, M.L. Di Giacinto, L. Cristaldi, D. Nuzzo, C. Dispenza, D. Giacomazza, M. Di Carlo, Ionizing radiation-engineered nanogels as insulin nanocarriers for the development of a new strategy for the treatment of Alzheimer's disease, Biomaterials 80 (2016) 179–194.
[19] P. Picone, D. Nuzzo, L. Caruana, E. Messina, A. Barera, S. Vasto, M. Di Carlo, Metformin increases APP expression and processing via oxidative stress, mitochondrial dysfunction and NF-κB activation: use of insulin to attenuate metformin's effect, Biochim. Biophys. Acta 1853 (2015) 1046–1059.
[20] P. Morell, R.H. Quarles, et al.G.J. Siegel, B.W. Agranoff, R.W. Albers Basic, et al. (Eds.), Characteristic composition of myelin, Neurochemistry: Molecular, Cellular and Medical Aspects (1999).
[21] A. Bruinink, R. Luginbuehl, Evaluation of biocompatibility using *in vitro* methods: interpretation and limitations, Adv. Biochem. Eng. Biotechnol. 126 (2012) 117–152.

[22] L.A. Keller, O. Merkel, A. Popp, Intranasal drug delivery: opportunities and toxicologic challenges during drug development, Drug Deliv. Transl. Res. 12 (2022) 735–757.
[23] E. Grajchen, E. Wouters, B. van de Haterd, M. Haidar, K. Hardonniere, T. Dierckx, J. Van Broeckhoven, C. Erens, S. Hendrix, S. Kerdine-Romer, J.J.A. Hendriks, J.F.J. Bogie, CD36-mediated uptake of myelin debris by macrophages and microglia reduces neuroinflammation, J. Neuroinflamm. 17 (2020) 224.
[24] G. Hammel, S. Zivkovic, M. Ayazi, Y. Ren, Consequences and mechanisms of myelin debris uptake and processing by cells in the central nervous system, Cell. Immunol. 380 (2022) 10459.
[25] Y. Liu, W. Hao, M. Letiembre, S. Walter, H.Neumann Kulang, K. Fassbender, Suppression of microglial inflammatory activity by myelin phagocytosis: role of p47-PHOX-mediated generation of reactive oxygen species, J. Neurosci. 13 (2006) 12904–12913.
[26] A. Henn, S. Lund, M. Hedtjärn, A. Schrattenholz, P. Pörzgen, M Leist, The suitability of BV2 cells as alternative model system for primary microglia cultures or for animal experiments examining brain inflammation, ALTEX 26 (2009) 83–94.
[27] K. Williams, E. Ulvestad, A. Waage, J.P. Antel, J. McLaurin, Activation of adult human derived microglia by myelin phagocytosis *in vitro*, J. Neurosci. Res. 38 (1994) 433–443.
[28] K. Mosley, M.L. Cuzner, Receptor-mediated phagocytosis of myelin by macrophages and microglia: effect of opsonization and receptor blocking agents, Neurochem. Res. 21 (1996) 481–487.
[29] L.J. Van der Laan, S.R. Ruuls, S. Weber, I.J. Lodder, E.A. Döpp, C.D. Dijkstra, Macrophage phagocytosis of myelin *in vitro* determined by flow cytometry: phagocytosis is mediated by CR3 and induces production of tumor necrosis, J. Neuroimmunol. 70 (1996) 145–152.
[30] L.A. Boven, M. Van Meurs, M. Van Zwam, A. Wierenga-Wolf, R.Q. Hintzen, R.G. Boot, J.M. Aerts, S. Amor, E.E. Nieuwenhuis, J.D. Laman, Myelin-laden macrophages are anti-inflammatory, consistent with foam cells in multiple sclerosis, Brain 129 (2006) 517–526.
[31] O. Butovsky, Y. Ziv, A. Schwartz, G. Landa, A.E. Talpalar, S. Pluchino, G. Martino, M. Schwartz, Microglia activated by IL-4 or IFN-gamma differentially induce neurogenesis and oligodendrogenesis from adult stem/progenitor cells, Mol. Cell. Neurosci. 31 (2006) 149–160.
[32] O. Butovsky, A.E. Talpalar, K. Ben-Yaakov, M. Schwartz, Activation of microglia by aggregated beta-amyloid or lipopolysaccharide impairs MHC-II expression and renders them cytotoxic whereas IFN-gamma and IL-4 render them protective, Mol. Cell. Neurosci. 29 (2005) 381–393.
[33] C. Rossi, M. Cusimano, M. Zambito, A. Finardi, A. Capotondo, J.M. Garcia-Manteiga, G. Comi, R. Furlan, G. Martino, L. Muzio, Interleukin 4 modulates microglia homeostasis and attenuates the early slowly progressive phase of amyotrophic lateral sclerosis, Cell Death Dis. 14 (2) (2018) 250 9.
[34] S. Mori, P. Maher, B. Conti, Neuroimmunology of the Interleukins 13 and 4, Brain Sci. 13 (2) (2016) 18 6.
[35] M. Falcone, A.J. Rajan, B. Bloom, C.F. Brosnan, A critical role for IL-4 in regulating disease severity in experimental allergic encephalomyelitis as demonstrated in IL-4-deficient C57BL/6 mice and BALB/c mice, J. Immunol. 15 (1998) 4822–4830.
[36] M.F. Dumont, S. Yadavilli, R.W. Sze, J. Nazarian, R. Fernandes, Manganese-containing Prussian blue nanoparticles for imaging of pediatric brain tumors, Int. J. Nanomed. 23 (2014) 2581–2595.
[37] H. Xia, X. Gao, G. Gu, Z. Liu, N. Zeng, Q. Hu, Q. Song, L. Yao, Z. Pang, X. Jiang, J. Chen, H. Chen, Low molecular weight protamine-functionalized nanoparticles for drug delivery to the brain after intranasal administration, Biomaterials 32 (2011) 9888–9898.
[38] B. Hemmer, J.J. Archelos, H.P. Hartung, New concepts in the immunopathogenesis of multiple sclerosis, Nat. Rev. Neurosci. 3 (2002) 291–301.
[39] L. Steinman, Multiple sclerosis: a coordinated immunological attack against myelin in the central nervous system, Cell 85 (1996) 299–302.
[40] V.V. Ivanova, S.F. Khaiboullina, M.O. Gomzikova, E.V. Martynova, A.M. Ferreira, E.E. Garanina, D.I. Sakhapov, Y.A. Lomakin, T.I. Khaibullin, E.V. Granatov, F.A. Khabirov, A.A. Rizvanov, A. Gabibov, A. Belogurov, Divergent immunomodulation capacity of individual myelin peptides-components of liposomal therapeutic against multiple sclerosis, Front. Immunol. 16 (2017) 1335.
[41] F. Navabi, V. Shaygannejad, F. Abbasirad, E. Vaez, F. Hosseininasab, M. Kazemi, O. Mirmosayyeb, F. Alsahebfosoul, N. Esmaeil, Immunoregulatory effects of silymarin on proliferation and activation of Th1 cells isolated from newly diagnosed and IFN-ß1b-treated MS patients, Inflammation 42 (2019) 54–63.
[42] A.W. Smith, B.P. Doonan, W.R. Tyor, N. Abou-Fayssal, A. Haque, N.L. Banik, Regulation of Th1/Th17 cytokines and IDO gene expression by inhibition of calpain in PBMCs from MS patients, J. Neuroimmunol. 232 (2011) 179–185.
[43] T. Crowley, J.M. Fitzpatrick, T. Kuijper, J.F. Cryan, O. O'Toole, O.F. O'Leary, E.J. Downer, Modulation of TLR3/TLR4 inflammatory signaling by the GABAB receptor agonist baclofen in glia and immune cells: relevance to therapeutic effects in multiple sclerosis, Front. Cell. Neurosci. 28 (2015) 284.
[44] R.D. Hollifield, L.S. Harbige, D. Pham-Dinh, M.K. Sharief, Evidence for cytokine dysregulation in multiple sclerosis: peripheral blood mononuclear cell production of pro-inflammatory and anti-inflammatory cytokines during relapse and remission, Autoimmunity 36 (2003) 133-14.
[45] T.F. Gajewski, S.R. Schell, G. Nau, F.W. Fitch, Regulation of T-cell activation: differences among T-cell subsets, Immunol. Rev. 111 (1989) 79–110.
[46] Z. Sternberg, K. Chadha, A. Lieberman, A. Drake, D. Hojnacki, B. Weinstock-Guttman, F. Munschauer, Immunomodulatory responses of peripheral blood mononuclear cells from multiple sclerosis patients upon *in vitro* incubation with the flavonoid luteolin: additive effects of IFN-beta, J. Neuroinflamm. 13 (2009) 28.
[47] P.B. Vani, V. Chitra, The role of the proinflammatory and anti-inflammatory cytokines in multiple sclerosis, Biomed. Pharmacol. J. 15 (2022) 137–146.
[48] M.F. Bachmann, G.T. Jennings, Vaccine delivery: a matter of size, geometry, kinetics and molecular patterns, Nat. Rev. Immunol. 10 (2010) 787–796.
[49] V. Manolova, A. Flace, M. Bauer, K. Schwarz, P. Saudan, M.F. Bachmann, Nanoparticles target distinct dendritic cell populations according to their size, Eur. J. Immunol. 38 (2008) 1404–1413.
[50] K. Fytianos, L. Rodriguez-Lorenzo, M.J. Clift, F. Blank, D. Vanhecke, C. von Garnier, A. Petri-Fink, B. Rothen-Rutishauser, Uptake efficiency of surface modified gold nanoparticles does not correlate with functional changes and cytokine secretion in human dendritic cells *in vitro*, Nanomedicine 11 (2015) 633–644.
[51] W. Yan, W. Chen, L. Huang, Reactive oxygen species play a central role in the activity of cationic liposome based cancer vaccine, J. Control. Release 130 (2008) 22–28.
[52] A. Cifuentes-Rius, A. Desai, D. Yuen, A.P.R. Johnston, N.H. Voelcker, Inducing immune tolerance with dendritic cell-targeting nanomedicines, Nat. Nanotechnol. 16 (2021) 37–46.